Radiography System Optimization Using Multi-objectives Particle Swarm Optimization

Robert Nshimirimana *, [a, c], Ajith Abraham[b], Gawie Nothnagel[c]

[a] *Department of Computer Science, University of Pretoria, South Africa,*

[b] *Machine Intelligence Research Labs (MIR Labs), Scientific Network for Innovation and Research Excellence Auburn, Washington 98071, USA,*

[c] *Radiation Science Department, South African Nuclear Energy Corporation SOC Ltd, South Africa,*

[*] *Corresponding Author:*

Email address: robert.nshimirimana@necsa.co.za

ABSTRACT

Radiography is a 2-D transmission imaging technique that is extensively used for non-destructive investigation of materials. The integrity of the investigation depends on the quality of the radiographic image, and the quality of the radiograph can be improved by arranging the radiography system parameters in such a way that it approaches a compromised optimum for a given application. Radiography system optimization is a real life multi-objective optimization problem, and a manual approach to optimization is a time consuming, labour intensive process, and prone to human error. In this paper, an optimization approach based on a simplified radiography simulator coupled to a multi-objective particle swarm optimization routine is described. For any given set of scanning (system) parameters the simulator produces a virtual radiograph from which quality factors can be derived, while the optimizer make use of these quality factors to search for the best design parameters or scanning parameters for a radiography system. The radiography system optimizer was successfully tested and benchmarked against experimental results. The benchmark test results showed that the optimizer was able to provide a set of Pareto optimal solutions from which scanning or design parameters can be retrieved to optimize a real radiography system.

Keywords:

Multi-objective optimization, Radiography system, particle swarm, image quality.

1. Introduction

A radiography system (RS) is used to perform a 2-D projection imaging technique for non-destructive investigation to retrieve qualitative and quantitative information of the internal structure of a sample under investigation[1, 2]. The integrity of the investigation lies partly in the quality of a radiograph measured using different quality parameters such as contrast, penetration, sharpness, and resolution. These radiographic qualities are in conflict with one another; therefore, optimization of a radiography scanning system is a real life multi-objectives optimization problem (MOOP). The MOOP for a RS is solved by finding the best scanning parameters that produce a quality radiograph for a particular radiography scan. In case an existing RS may not be suitable to produce an optimal quality radiograph desirable for a given investigation, an optimized custom designed RS need to be constructed to cater for the needs dictated for by the specific application. The empirical method of solving a MOOP for a RS implies changing the scanning parameters until a desired image quality is achieved. However, the empirical method is a time consuming, labour intensive process, which is prone to human error. For this reason a multi-objectives RS optimizer is an important tool to assist with the optimization of the geometric design of a new customized RS or of a particular scanning experiment.

Particle swarm optimization (PSO) is a population-based optimization approach based on swarm intelligence that was first introduced by Kennedy and Eberhart in 1995 [3]. PSO is an efficient and simple to implement optimization algorithm [4-6]. PSO has a quick convergent rate to a solution[7, 8]. Multi-objective algorithms based on PSO (MOOPSO) have been successfully used to solve real life optimisation problems [9-11]. Despite their success, the performance of a MOOPSO is problem dependent [11-16] and that create the need to find a suitable MOOPSO for radiography optimization problem. Looking among existing MOOPSO is a challenge because existing MOOPSO are tailored to solve a particular real life multi-objective optimization problem, and there is ongoing effort to improve the performance of the existing MOOPSO. Finding a suitable MOOPSO for radiography optimization problem requires the modification of the existing MOOPSO or the design of the new MOOPSO.

This paper presents a RS optimizer that uses a MOOPSO called MOPRAD to automatically provide Pareto optimal solutions to a radiography optimization problem found in a neutron and X-ray RS. The optimizer is designed to optimize the geometric or functional aspects of the main components of a RS. The optimization process is done in a virtual RS to automatically search for the best parameters for the design or scanning for a real RS. The optimizer can be used during the design phase or during the operations of a RS. The MOPRAD is based on Coello Coello and Lechuga MOOPSO algorithm [16].The MOPRAD can solve unconstraint and constraint real life radiography optimization problem. The MOPRAD uses constant PSO control parameters throughout the optimization process.

The remainder of this paper is organized as follows. Section 2 discusses the application of ray tracing in RS modelling, and the integration of an image quality calculator into the simulator. Section 3 presents the results of different benchmark tests for the simulator. Finally, the conclusions and findings are presented in section 4.

2. Multi-objectives optimization problem for radiography system

A RS is used in the investigation of the internal structure of the sample. It is imperative to optimize the design or set-up parameters of the RS to produce a high quality radiograph. An ideal quality radiograph should have a high contrast, high spatial resolution, high beam penetration, and high sharpness as illustrated in the figure below:

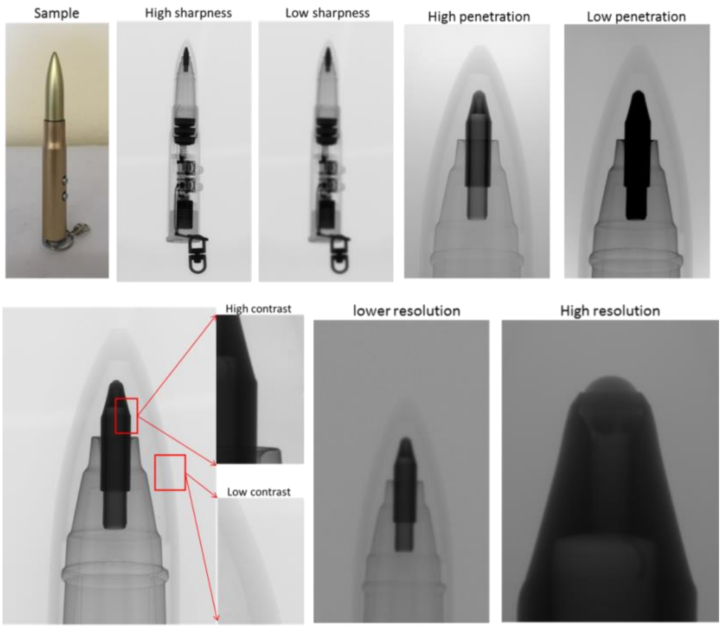

Figure 1: Effect of quality factors in a radiograph.

Figure 1 depicts the effect of quality factors on a radiographic image of a pen. A lack of contrast in a radiographic image translates to a lack of quality of information from a radiograph [17-20], the is desired in a radiograph in order to have high definition of details within the radiograph [21-23], the beam penetration contributes to the amount of information available on the radiograph [24-27], and a radiograph with high resolution contains great detail of information and allows visualization of fine details the sample under investigation [28-31].

The objectives of an ideal quality radiograph are in conflict with each other. A high beam penetration may lead to a lower contrast in the radiograph, and a high spatial resolution may create a lower sharpness in the radiograph. A trade-offs between the conflicting objectives is needed in the RS optimization. This makes a RS optimization a multi-objectives optimization problem. In this study, a general multi-objectives optimization problem for a RS is defined as follow:

$$Optimize\ \vec{f}_{rad}(\vec{p}_{rad}) \quad subject\ to \tag{1}$$

$$q_j(\vec{p}_{rad}) \geq c_j \qquad j = \{contrast, penetration, \dots, n\} \tag{2}$$

$$p_{min} \leq p_i \leq p_{max} \qquad i = \{1,2,3, \ \dots, m\} \tag{3}$$

where $\vec{f}_{rad} = (f_{contrast}, f_{penetration}, \dots, f_n)$ is vector function representing the objective functions for RS optimization, f_n is an objective function for n quality factor of a radiograph, $\vec{p}_{rad}$ is a vector of decision variables representing the set-up parameters or design parameters of a RS, q_j is the inequality constraint function, c_j is the constraint value for objective j, p_{min} and p_{max} are the lower and upper boundaries respectively for decision variable p_i.

3. Pareto Optimal solutions

The MOOP for a RS was solved as a set of Pareto-optimal solutions (Figure 2). The Pareto optimal solutions are solutions that have good compromises between the objectives. Pareto-optimal solutions concept has been the most preferable choice for evolutionary and swarm intelligence algorithms in solving a MOOP [32, 33].

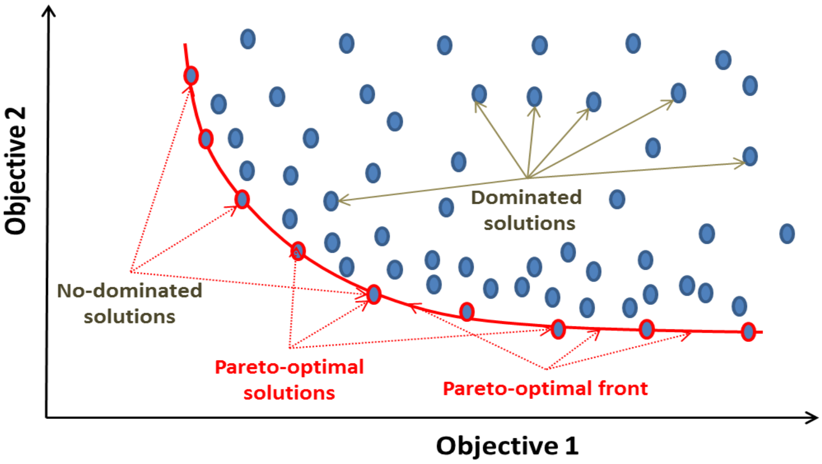

Figure 2: Illustration of Pareto optimal solutions.

Pareto solutions use a concept of “domination”. A solution found by a particle in a search space of a MOOP can be either classified as a “dominated solution” or a “nondominated solution”. A dominated solution is a solution whose one or more objectives can be improved without causing damage to others objectives in the same solution. A nondominated solution is a solution whose objectives cannot be improved without degrading other objectives [33-35]. A Pareto optimum solution is a nondominated solution.

A RS optimizer was designed to provide Pareto optimal solutions to the MOOP for a RS. The optimizer is made of a radiography simulator (not discussed here) that provides a virtual environment, and an optimization algorithm that automatically searches for the solutions in a virtual environment. The flowchart of the optimizer is illustrated below:

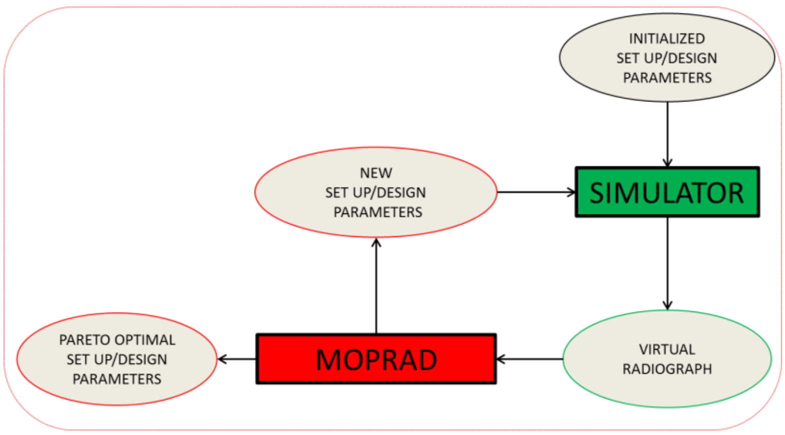

Figure 3: Flowchart of the radiography system optimization.

The process of optimization is depicted in Figure 3; the process starts with the MOOPSO providing the randomly initialized parameters to the simulator for quality testing. The simulator simulates a radiograph based on the parameters provided by the MOOPSO. The quality factors of the simulated radiograph (virtual radiograph) are fed into the MOOPSO which provides new parameters for test in the simulator and the process repeats again. The process ends when the defined number of loops (time step) is reached, in which case a Pareto optimal front alongside a Pareto optimal solutions are provided.

4. Algorithm

The multi-objectives particle swarm algorithm proposed for radiography optimization is based on the Coello Coello and Lechuga algorithm called MOPSO [16]. The MOPSO has been modified to solve unconstraint and constraint real life optimization problems found in RS optimization. The constraint handling mechanisms such as death penalty are used in the MOPRAD to keep the particles in the feasible search space. The velocity clamping technique is used in the MOPRAD to prevent particle explosion. A Gaussian mutation operator is used to diversify the Pareto optimal solutions. During the search of the optimal solution, the velocity of each particle in the swarm is updated using

$$v_i^a(t+1) = \omega v_i^a(t) + r_{1i}^a(t) c_1 \left[x_i^y(t) - x_i^a(t)\right] + r_{2i}^a(t)\, c_2 \left[\hat{x}_i^y(t) - x_i^a(t)\right] \tag{4}$$

where v_i^a is the velocity of the particle a for i parameter at time t, ω is the inertia weight, r_{1i} and r_{2i} are random values in $[0,1]$ for the particle a for i parameter, c_1 and c_2 are acceleration coefficients, x_i^y is the local guide for particle a for i parameter, x_i^a is the current position of particle a for i parameter, and $\hat{x}_i^y(t)$ is the global guide for all particles for i parameter. To conserve the stochastic nature of the algorithm, new random numbers for r_1, r_2 are generated for each parameter at each iteration.

The position of the particles is updated using

$$x_i^a(t+1) = \varphi_{G_i}^a(t) x_i^a(t) + v_i^a(t+1) \tag{5}$$

where x_i^a is the position of the particle a, and $\varphi_{G_i}^a$ is the generated Gaussian mutation operator for particle a and i parameter. $\varphi_{G_i}^a$ is used randomly on selected particles and the probability of the using $\varphi_{G_i}^a$ decreases at each time step.

The flowchart diagram of the MOPRAD is shown below

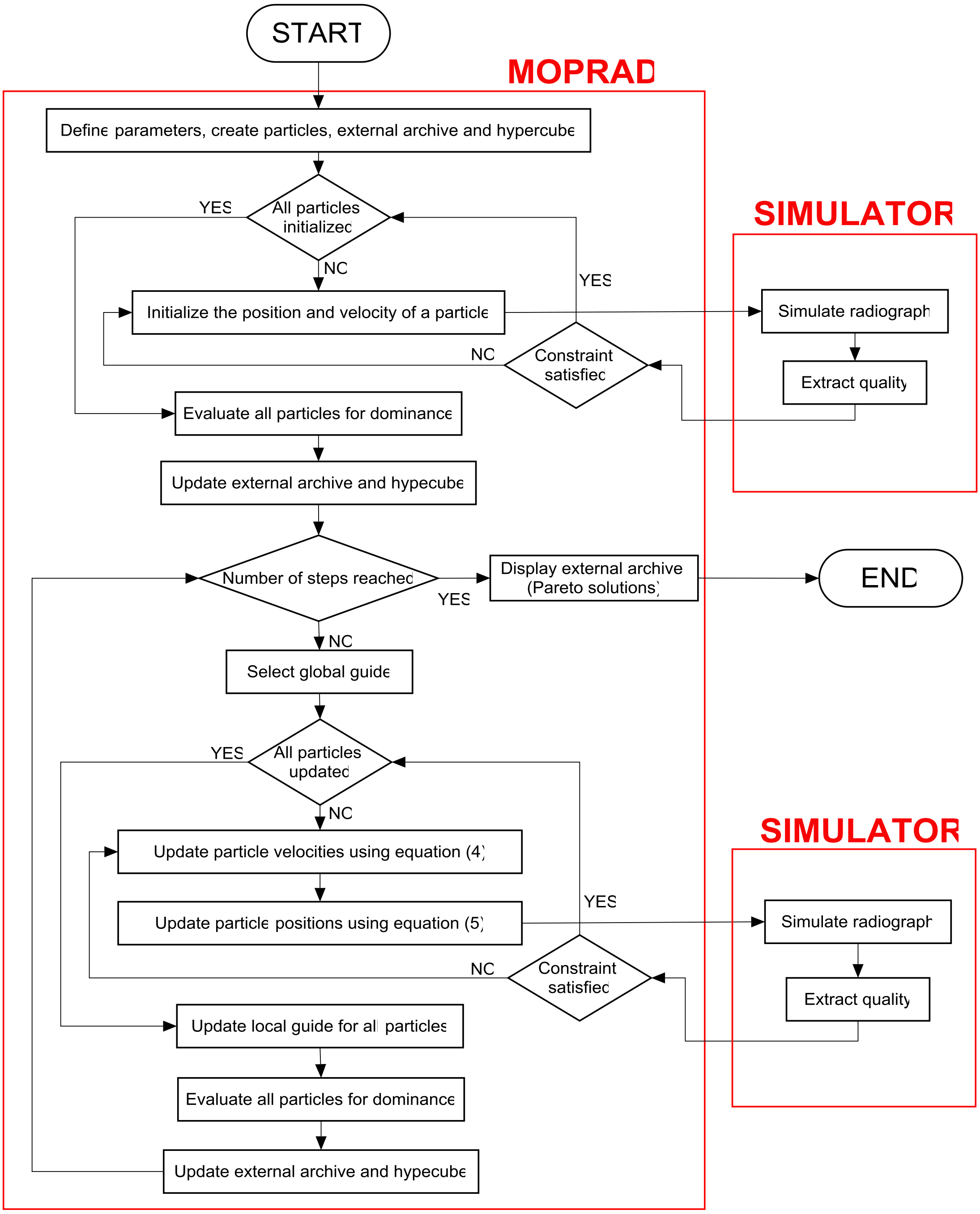

Figure 4: Flowchart diagram of the MOPRAD.

The optimization is done in a virtual environment representing an X-ray/neutron radiography system. The virtual environment is created using a radiograph simulator, and calibrated from experimental data taken using a real radiography system. The calibration process makes a simulated radiograph from the model comparable to the real radiograph. This is required for the integrity of the optimization results. The MOPRAD run the optimization in a calibrated virtual environment taking into account all the constraints parameters. At the end of the run a solution to the RS optimization problem is provide in a form of a Pareto-optimal front with the corresponding of Pareto optimal solutions. Only one solution is chosen among the set of Pareto-optimal solutions. The choice of the solution depends on the decision maker's preferences and the trade-off of the quality characteristics of the radiograph. Several approaches such as clustering and ranking have been proposed for the selection of the ideal solution among the Pareto optimal solutions [36-40].

5. Test and results

The effectiveness of the optimizer was tested in two categories of real life RS optimization problems. The first category is the optimization of the set-up parameters before an X-ray radiography scan is conducted. The second category is the optimization of the geometric design of neutron radiography collimator. The solutions for both categories were presented in form a Pareto optimal front. The results of the optimization were verified using a real microfocus X-ray radiography system or by simulation.

The optimizations were run with the PSO parameters in Table 1.

Table 1: PSO parameters used in the optimization

PSO PARAMETERS	VALUE
Accelerator coefficient ($C1$)	1.4
Accelerator coefficient ($C2$)	1.4
Inertia weight (ω)	0.7
Number of particles	100
Number hypercubes in the external archive	30
The size of the external archive	250
Mean for Gaussian mutation operator	0
Coefficient of the Velocity clamping function	1
Number of time steps	250

5.1. Optimization of an X-ray radiography scan

The objective of the optimization is to find the best set-up parameters for a microfocus X-ray radiography scan. The set-up parameters to optimize are from the three main components of a microfocus X-ray radiography system namely the X-ray source, the sample under investigation, and the X-ray detection as illustrated below:

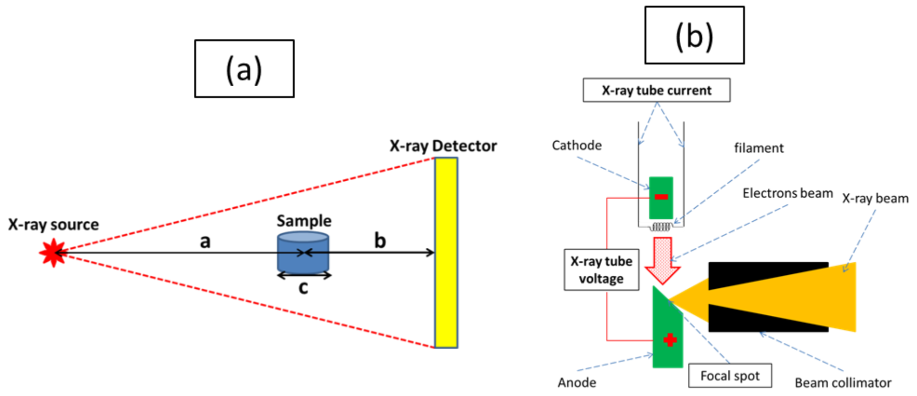

Figure 5: Illustration of a microfocus X-ray radiography system (a) and X-ray source (b).

The set-up parameters of each component need to be fine-tuned to produce the best possible quality radiograph of the sample under investigation. The current method of finding the best parameters involves a manual procedure in which the operator searches the best parameters by manipulating various set-up parameters of each component of microfocus X-ray radiography system. The manual procedure is time consuming and is prone to error.

The position and the parameters of each component have an influence to the quality of a radiograph. The quality of a radiograph was evaluated in term of contrast, unsharpness and effective pixel size. The decision variables parameters were chosen based on the set-up parameters that need to be fine-tuned in the experiment. The objectives were chosen based on the image quality parameters that need to be optimized. The decision variables and the objectives used in the optimization are shown in table below:

Table 2: Decision variables and objectives for X-ray set-up scan optimization

DECISION VARIABLES	OBJECTIVES
X-ray tube voltage (V)	Contrast
X-ray tube current (J)	Unsharpness
Exposure time (t)	Effective pixel size
Sample position (z)	

The objective function to optimize was defined in (6) as:

$$Optimize\ \vec{f}_{rad}(\vec{p}_{rad}) = S_{rad}(\vec{p}_{rad}) \tag{6}$$

where $\vec{f}_{rad} = (f_{contrast}, f_{unsharpness}, f_{effective\ pixel})$ is vector function representing the objective functions, $\vec{p}_{rad} = (V, J, t, z)$ is a vector of decision variables representing the set-up parameters, and S_{rad} is a simulator function.

The verification of the optimization was done using a microfocus X-ray machine with each Pareto optimal solutions as set-up parameters for the scan. Two metal samples and a microfocus X-ray radiography system [41] situated at Necsa [42] shown in Figure 6 were used in the test.

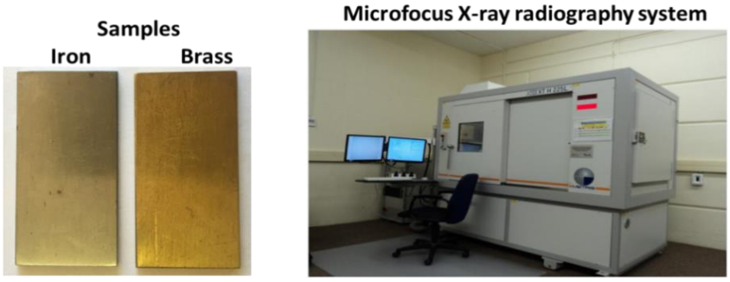

Figure 6: Samples and a microfocus X-ray radiography system used in the test.

The results of the test are shown in Figure 7. Each point in the graph in Figure 7 represents a vector solution (shown in Table 3 and Table 4 in the appendix) of the best scanning set-up parameters. The verification results showed an average error of 0.47% and a standard deviation of 0.23% between the optimization and the experimental results for a two objectives optimization (effective pixel size vs unsharpness). For three objectives optimization (contrast vs effective pixel size vs unsharpness), the verification results showed an average error of 2.18% with a standard deviation of 2.13% between the optimization and the experimental results.

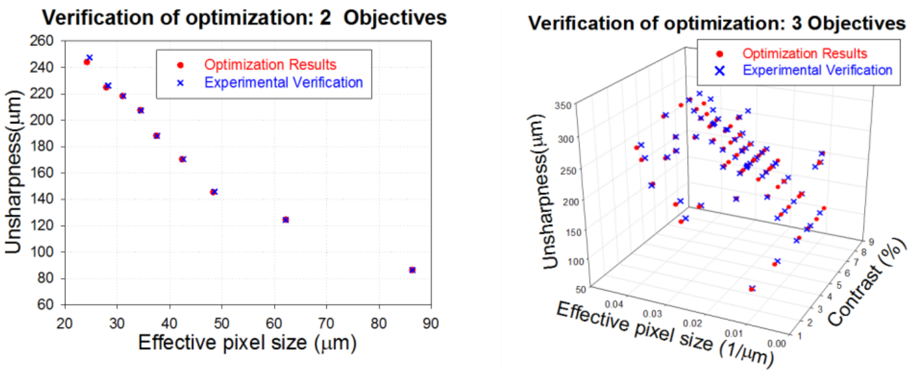

Figure 7: Optimization results and verification using a microfocus X-ray machine.

5.2. Optimizing the geometric design of a neutron radiography collimator

The objective of the optimization is to find the best size and the best position of the collimator aperture that provide the ideal neutron radiography beam. The ideal neutron radiography beam should have a large area of homogeneity, a high neutron flux at the detector position, and be able to produce a high resolution radiograph. A large area of homogeneity provides a large field of view, allows the investigation of bigger samples, and quantitative analysis. A high neutron flux gives better contrast, and gives the possibility of shortening the time for the neutron scan.

The optimization problem of a neutron collimator was defined in term of the diameter D and the position L of the aperture relative to the detector (assuming the sample is placed at the detector position). The L/D ratio characterizes the ideal neutron beam. A suitable values of D and L are needed to balance the need of high resolution, high field of view, and high contrast in the radiograph. The optimization was conducted by considering decision variables as the size D of the diameter of the aperture, and the position L of the aperture position with respect to the neutron detector. The objectives of the optimization function were the neutron flux and the area of homogeneity. The maximum gray value G_v and the radius of beam homogeneity R_h were used to measure the neutron flux and the area of homogeneity respectively. The objective function to optimize was defined in (6) as:

$$Optimize\ \vec{f}_{rad}(\vec{p}_{rad}) = S_{rad}(\vec{p}_{rad}) \tag{7}$$

where $\vec{f}_{rad} = (f_{G_v}, f_{R_h})$ is vector function representing the objective functions, $\vec{p}_{rad} = (D, L)$ is a vector of decision variables representing the design parameters, and S_{rad} is a simulator function.

The test was done on the design of a neutron radiography collimator at the beam tube 2 situated at the SAFARI-1 nuclear research reactor at Nesca. The geometry of the beam tube 2 with the parameters D and L is illustrated below:

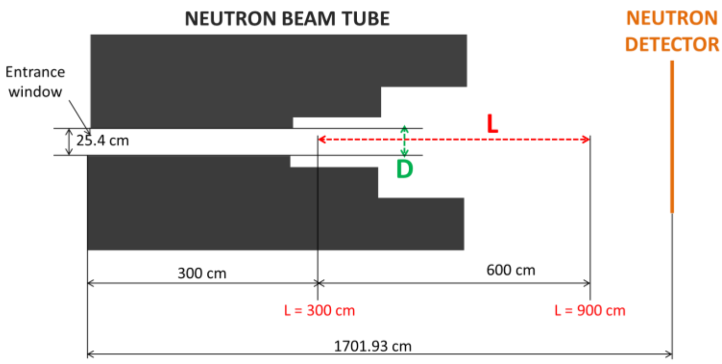

Figure 8: Illustration of the geometry of the beam tube 2 at the SAFARI-1 nuclear research reactor.

The results of optimization are presented below:

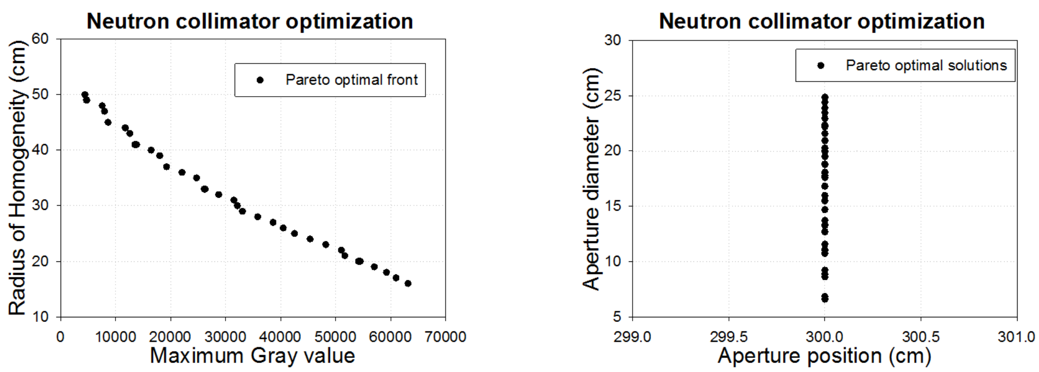

Figure 9: Pareto optimal front (right) and the corresponding Pareto optimal solutions (left) for neutron radiography collimator.

The 300 cm position taken by all the solutions in Figure 9 are in the lower boundary of the search space (refer Figure 8), and it is closest position from the neutron source. Further analyses were conducted to confirm if the optimization solutions favour the aperture position that is the closest to the neutron source. The analyses were done by repeating the neutron collimator optimization with different search ranges. The results of the analysis are shown in the figure below:

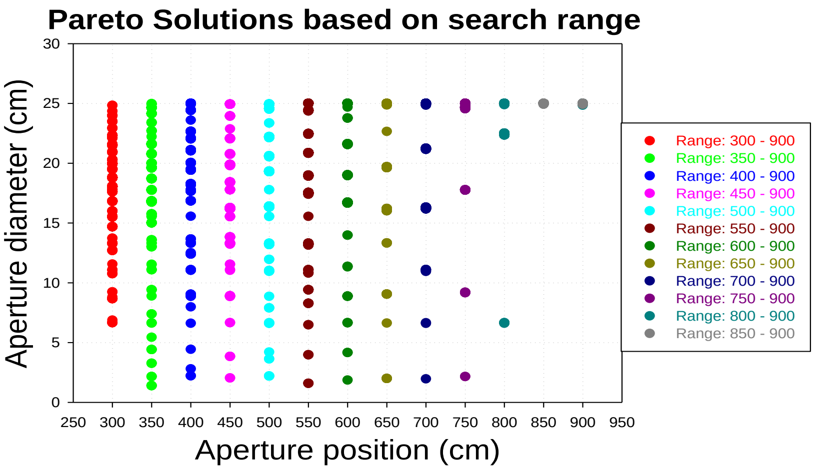

Figure 10: Pareto optimal solutions obtained from different ranges of search space

The results in Figure 10 confirmed that all the Pareto optimal solutions provide the aperture position at the lower bound of the search range. The lower bound of the search range is the closest position to the neutron source. The results also show that the number of possible optimal solutions decreased as the search range moves further away from the neutron source.

A verification of the neutron collimator optimization results was done using the line profile analysis technique to verify the measurement of the radius of homogeneity and maximum gray value (neutron flux) from the resulted simulated radiographs. The radiographs were simulated using five optimal L/D ratio from the Pareto optimal solutions. The results of verification are shown below:

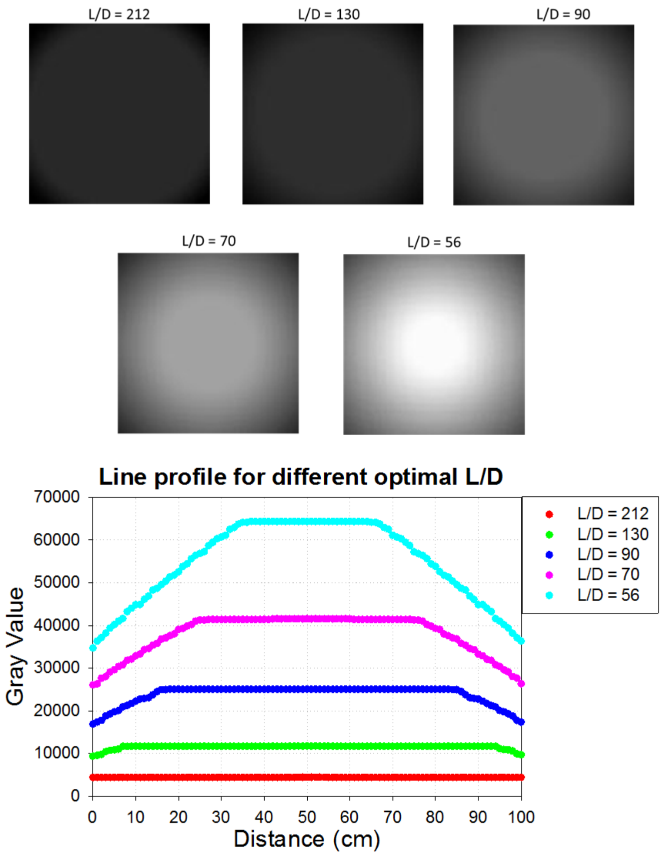

Figure 11: Simulated radiograph and line profile analysis of five Pareto optimal solutions.

The verification results show an average error of 1.08% with a standard deviation of 1.59% between the values of the radius of homogeneity from the Pareto optimal solutions and the line profile analysis. An average error of 1.33% with a standard deviation of 0.89% was observed between the values of the maximum gray value from Pareto optimal solutions and the line profile analysis.

6. Conclusion

The optimization problems of a radiography system were successfully solved using a multi-objectives particle swarm optimization in a virtual environment representing an X-ray and a neutron radiography system. The MOPRAD provides Pareto optimal solutions within which one solution can be selected by the operator to optimize a radiography scan or a design of a radiography system. The solutions provided by the MOPRAD were successfully verified experimentally using a microfocus X-ray radiography system and by simulation. The results of the optimization of the geometric parameters for a neutron radiography collimator showed that the collimator aperture position should be as close as possible to the radiation source. Future work will focus on integration of parallel computing in the optimizer to further improve computational time. A many-objectives optimization algorithm should be also be considered.

Acknowledgements

The author wishes to thank the support of the South African Nuclear Energy Corporation (Necsa) and the National Research Foundation (NRF). The author is deeply grateful to the Radtom section at Necsa for the support during execution of this work.

Reference

[1] E. Hussein, *Introduction. In Handbook on radiation probing, gauging, imaging and analysis.* Springer, 2003.

[2] D. A. Lisle, *Introduction to medical imaging. In Imaging for students.* CRC Press, 2012.

[3] J. Kennedy and R. C. Eberhart, "Particle Swarm Optimization," in *The IEEE International Joint Conference on Neural Networks*, Perth, 1995, pp. 1942–1948, New Jersey: IEEE, 1995.

[4] A. P. Engelbrecht, "Particle Swarm Optimization," in *Computational Intelligence: An Introduction*West Sussex, England: John Wiley & Sons Ltd, 2007, pp. 289-357.

[5] Q. Bai, "Analysis of Particle Swarm Optimization Algorithm," *Computer and Information Science*, vol. 3, no. 1, pp. 180-184, 2010.

[6] K. Boudjelaba, F. Ros, and D. Chikouche, "Potential of Particle Swarm Optimization and Genetic Algorithms for FIR Filter Design," *Circuits Syst Signal Process*, vol. 33, no. 2014, pp. 3195–3222, 2014.

[7] Geetika and J. Singh, "Hybridization of Particle Swarm Optimization - A Survey," *International Journal of Science and Research*, vol. 4, no. 1, pp. 2417-2420, 2015.

[8] R. Thangaraj, M. Pant, A. Abraham, and P. Bouvry, "Particle swarm optimization: Hybridization perspectives and experimental illustrations," *Applied Mathematics and Computation*, vol. 217, no. 12, pp. 5208–5226, 2011.

[9] S. Lalwani, S. Singhal, R. Kumar, and N. Gupta, "A Comprehensive Survey: Applications of Multi-Objective Particle Swarm Optimization (Mopso) Algorithm," *Transactions on Combinatorics*, vol. 2, no. 1, pp. 39-101, 2013.

[10] N. K. Kulkarni, S. Patekar, T. Bhoskar, O. Kulkarni, G. M. Kakandikar, and V. M. Nandedkar, "Particle Swarm Optimization Applications to Mechanical Engineering- A Review," *Materials Today: Proceedings*, vol. 2, no. 2015, pp. 2631 – 2639, 2015.

[11] Y. Zhang, S. Wang, and G. Ji, "A Comprehensive Survey on Particle Swarm Optimization Algorithm and Its Applications," *Mathematical Problems in Engineering*, vol. 2015, no. 1, pp. 1-38, 2015.

[12] V. Kumar and S. Minz, " Multi-objective particle swarm optimization: An Introduction," *Smart Computing Review*, vol. 4, no. 5, pp. 335-353, 2014.

[13] M. Reyes-Sierra and C. A. C. Coello, "Multi-Objective Particle Swarm Optimizers:A Survey of the State-of-the-Art," *International Journal of Computational Intelligence Research*, vol. 2, no. 3, pp. 287–308, 2006.

[14] A. Atyabi and S. Samadzadegan, "Particle Swarm Optimization : A Survey," in *Applications of Swarm Intelligence*, L. P. Walters, Ed. New York, UK: Nova Science Publishers, 2011, pp. 167 -179.

[15] A. R. Jordehi and J. Jasni, "Parameter selection in particle swarm optimisation: a survey," *Journal of Experimental & Theoretical Artificial Intelligence*, vol. 25, no. 4, pp. 527-542, 2013.

[16] C. A. C. Coello, G. T. Pulido, and M. S. Lechuga, "Handling Multiple Objectives With Particle Swarm Optimization," *IEEE Transactions on Evolutionary Computation*, vol. 8, no. 3, pp. 256-279, 2004.

[17] S. S. Hiss, "Charateristics of the radiographic image," in *Understanding radiography*4 ed. Springfield: Charles C Thomas, 2003, pp. 3-28.

[18] M. Sandborg, "Radiography and Flouroscopy: Physical principles and biohazards," Linköping University LinköpingLIU-RAD-R-080 1995, vol. 80.

[19] B. Hasegawa, "Physical Determination of Contrast," in *Physics of Medical X-Ray Imaging*2 ed. Madison: Medical Physics Pub Corp, 1987, pp. 53-78.

[20] F. Campeau and J. Fleitz, "Fundamentals of Radiographic Exposure," in *Limited Radiography*3 ed. New York: Delmar Cengage Learning, 2009, pp. 233-269.

[21] J. Johnston and T. L. Fauber, "Image Quality and Characteristics," in *Essentials of Radiographic Physics and Imaging*Missouri: Elsevier, 2015, pp. 92-116.

[22] A. S. Whitley, C. Sloane, G. Hoadley, and A. D. Moore, "Basic Principles of Radiography and Digital Technology," in *Clark's Positioning in Radiography*Boca Raton: CRC Press, 2005, pp. 1-36.

[23] R. V. Daele, I. Verpoest, and P. De Meester, "Detection of Damage in Composite Materials Using Radiography," in *Manual on Experimental Methods for Mechanical Testing of Composites*London: Elsevier Applied Science, 1989, pp. 115-128.

[24] J. P. Barton, "Neutron Radiography-An Overview," in *Practical application of neutron radiography and gaging*Philadelphia: American Society for Testing and Materials STP 586, 1976, pp. 5-19.

[25] L. M. Lavin, "Radiographic Technique Evaluation," in *Radiography in Veterinary Technology*Missouri: Saunders Elsevier, 2007, pp. 89-96.

[26] R. Halmshaw, "Interpretation of radiographs," in *Industrial Radiology: Theory and practice*: Chapman & Hall, 1995, pp. 207-236.

[27] R. A. Ehrlich and D. M. Coakes, "Image Quality Factors," in *Patient Care in Radiography: With an Introduction to Medical Imaging*: Mosby, 2012, pp. 23-35.

[28] I. D. Robertson and D. E. Thrall, D. E. Thrall, Ed. *Textbook of Veterinary Diagnostic Radiology*, 6 ed. Missouri: Saunders, 2012.

[29] F. Campeau and J. Fleitz, "Digital Radiography and Picture Archiving and Communication Systems (PACS)," in *Limited Radiography*: Delmar Cengage Learning, 2009, pp. 271-286.

[30] T. M. Link, "Structure Analysis Using High Resolution Imaging Techniques," in *Radiology of Osteoporosis*: Springer, 2001, pp. 153-166.

[31] M. Berry, V. Chowdhury, S. Suri, and S. Mukhopadhyay, "Advance in CT Technology," in *Diagnostic Radiology: Advances in Imaging Technology*: Jaypee Brothers Medical Publishers, 2007, pp. 52-98.

[32] N. A. A. Aziz, A. W. Mohemmed, M. Y. Alias, and K. A. Aziz, "Particle Swarm Optimization for Constrained and Multiobjective Problems: A Brief Review," in *International Conference on Management and Artificial Intelligence*, Bali, 2011, vol. 6, pp. 146-150.

[33] K. Deb, "Multi-Objective Optimization," in *Multi-Objective Optimization using Evolutionary Algorithms*New York: Jhon Wiley & Sons, 2001, pp. 13-45.

[34] A. P. Engelbrecht, "Multi-Objective Optimization," in *Computational Intelligence: An Introduction*: John Wiley & Sons Ltd, 2007, pp. 569-574.

[35] C. A. C. Coello, G. B. Lamont, and D. A. V. Veldhuizen, "Basic Concepts," in *Evolutionary Algorithms for Solving Multi-Objective Problems*: Springer, 2007, pp. 1-57.

[36] S. Parisi, A. Blank, T. Viernickel, and J. Peters, "Local-utopia Policy Selection for Multi-objective Reinforcement Learning," in *IEEE Symposium Series on Computational Intelligence* Athens, 2016 pp. 1-7: IEEE
[37] V. M. Carrillo and H. Taboada, "A Sweeping Cones Technique for Post Pareto Analysis," in *2013 Industrial and Systems Engineering Research Conference*, Puerto Rico, 2013: Institute of Industrial Engineers.
[38] E. Zio and R. Bazzo, "A Comparison of Methods For Selecting Preferred Solutions in Multiobjective Decision Making," in *Computational Intelligence Systems in Industrial Engineering*, vol. 6, C. Kahraman, Ed. Amsterdam: Atlantis Press, 2012, pp. 23-43.
[39] P. M. Chaudhari, R. V. Dharaskar, and V. M. Thakare, "Computing the Most Significant Solution from Pareto Front obtained in Multi-objective Evolutionary," *International Journal of Advanced Computer Science and Applications*, vol. 1, no. 4, pp. 63-68, 2010.
[40] M. Cheikh, B. Jarboui, T. Loukil, and P. Siarry, "A Method for Selecting Pareto Optimal Solutions in Multiobjective Optimization," *Journal of Informatics and Mathematical Sciences*, vol. 2, no. 1, pp. 51-62, 2010.
[41] J. W. Hoffman and F. C. de Beer, "Characteristics of the Micro-Focus X-ray Tomography Facility (MIXRAD) at Necsa in South Africa," in *18th World Conference on Nondestructive Testing*, Durban, 2012: NDT.net, 2012.
[42] F. C. de Beer, "Characteristics of the neutron/X-ray tomography system at the SANRAD facility in South Africa," *Nuclear Instruments and Methods in Physics Research A*, vol. 542, pp. 1-8, 2005.

Appendix

Table 3: Results of the optimization and verification for three objectives

SOLUTION ID	PARETO OPTIMAL SOLUTIONS				OBJECTIVES (PARETO OPTIMAL FRONT)					
					CONTRAST (%)		EFFECTIVE PIXEL SIZE (µm)		UNSHARPNESS(µm)	
	Voltage (kV)	Current (µA)	Exposure Time (second)	Source Sample Distance (cm)	Optimization	Experimental verification	Optimization	Experimental verification	Optimization	Experimental verification
1	183.55	57.02	1.42	34.97	7.32	6.89	60.88	60.98	121.94	121.95
2	193.05	131.85	0.5	14.46	6.78	6.30	25.05	25.58	277.33	281.33
3	154.72	73.15	1.42	41.55	7.56	6.81	72.33	71.81	144.89	143.63
4	140.43	63.26	2	24.56	7.39	7.09	42.60	43.01	214.11	215.05
5	142.49	60.04	2	52.75	7.26	7.10	91.95	91.53	91.97	91.53
6	140	40	2	14	4.52	4.45	24.23	24.75	292.91	297.03
7	179.45	56.27	1.42	23.99	7.05	6.82	41.62	41.84	209.14	209.21
8	183.55	111.89	0.708	63.04	7.75	7.58	109.59	110.80	219.82	221.61
9	194.55	44.52	1.42	21.91	6.19	6.00	38.06	38.39	191.00	191.94
10	175.57	83.2	1	24.25	7.25	7.58	42.06	42.83	211.40	214.13
11	180.06	135.1	0.5	15.57	6.23	5.98	26.97	27.61	271.47	276.05
12	166.21	56.04	1.42	22.39	6.19	6.41	38.87	39.22	195.19	196.08
13	153.54	101.83	0.708	16.17	5.25	5.22	28.03	28.45	253.74	256.05
14	140	63.32	1	16.01	3.83	3.73	27.72	28.19	251.22	253.70
15	180.47	51.84	1.42	16.37	6.40	6.48	28.35	28.88	256.87	259.93
16	140	40	1	14.77	2.21	2.29	25.59	25.99	257.52	259.91
17	140	40	1	14.37	2.22	2.32	24.89	25.36	275.60	279.01
18	140	40	2.83	34.45	6.62	6.26	59.97	59.79	120.13	119.58
19	140	45.29	2.83	58.41	7.68	7.05	101.78	100.76	101.84	100.76
20	146.71	113.19	1	21.2	7.31	7.37	36.80	37.07	221.78	222.43
21	140	46.26	2.83	14	7.56	7.53	24.23	24.78	317.32	322.18
22	186.74	55.17	1.42	70.64	7.74	7.31	123.08	121.95	123.16	121.95
23	154.93	98.29	1	18.95	7.07	7.41	32.87	33.31	231.28	233.14
24	140	40	2.83	16.44	6.52	6.50	28.47	28.96	257.97	260.68
25	140	59.57	2	29.77	7.26	7.88	51.75	52.02	155.71	156.05
26	142.93	56.53	2	21.14	6.77	6.53	36.66	37.04	221.15	222.22
27	140	40	2.83	16.7	6.52	6.20	28.92	29.37	232.94	234.95
28	194.95	139.45	0.5	58.2	7.75	7.30	101.27	101.01	202.95	202.02
29	166.48	45.7	0.5	51.11	1.83	1.93	89.09	88.30	89.11	88.30
30	167.33	65.21	1.42	40.29	7.52	7.84	70.05	69.93	140.49	139.86
31	140	40	2.83	28.29	6.65	6.54	49.20	49.32	147.97	147.97
32	140	40	2.83	18.05	6.54	6.31	31.27	31.72	220.29	222.05
33	140	40	2.83	17.06	6.53	6.53	29.56	30.03	267.70	270.27
34	151.5	50.14	2	20.86	6.74	7.01	36.20	36.56	218.22	219.38
35	140	40	0.708	16.51	1.80	1.55	28.59	29.07	230.29	232.56
36	145.25	55.18	1.42	24.36	4.84	4.77	42.33	42.64	169.89	170.58
37	156.1	73.62	1.42	26.49	7.26	7.90	46.03	46.30	184.74	185.19
38	167.96	87.27	1	24.46	6.86	7.19	42.51	42.87	170.59	171.49
39	159.3	55.07	1.42	20.23	5.81	6.30	35.12	35.49	211.63	212.95
40	180.5	80.81	1	30.31	7.75	8.18	52.70	52.91	158.54	158.73
41	182.66	63.24	1	14.13	5.79	6.19	24.46	24.98	295.63	299.81
42	172.32	77.59	1	14.16	6.53	7.07	24.52	25.02	296.26	300.19
43	194.79	94.43	0.708	26.27	7.01	6.97	45.61	45.98	183.21	183.91
44	191.29	62.71	0.267	20.96	1.58	1.84	36.40	36.76	182.72	183.82
45	140	40	2.83	23.65	6.62	6.29	41.03	41.37	206.17	206.83
46	190.35	118.97	0.5	52.25	6.29	6.05	91.12	90.29	91.10	90.29
47	169.91	42.34	2	18.83	6.72	6.97	32.65	33.06	229.81	231.40
48	162.46	76.14	0.5	21.19	2.88	2.96	36.80	37.14	184.73	185.70
49	188.75	85.73	0.5	51.79	3.87	4.17	90.29	89.69	90.30	89.69
50	161.15	110.85	0.708	23.24	6.28	6.12	40.36	40.77	202.60	203.87
51	191.87	47.41	0.5	19.22	1.95	2.21	33.36	33.73	201.06	202.36
52	152.06	67.21	1.42	20.73	6.33	6.71	35.94	36.33	216.86	217.98
53	199.63	132.76	0.5	17.22	7.19	7.25	29.83	30.33	240.19	242.61
54	187.25	54.73	1.42	18.84	7.39	7.38	32.65	33.14	262.78	265.12
55	188.55	74.69	1	14.73	7.20	7.53	25.49	26.06	282.50	286.64
56	198.7	71.35	1	57.88	7.75	7.92	100.76	100.25	201.83	200.50
57	153.89	74.5	1.42	26.61	7.42	7.56	46.24	46.51	185.58	186.05
58	140	40	1.42	15.88	3.15	3.11	27.53	28.01	249.18	252.10
59	140	40	2.83	23.88	6.63	5.97	41.45	41.80	208.18	208.99
60	146.79	41.85	2.83	17.71	7.39	6.81	30.70	31.18	247.02	249.42
61	177.55	74.92	1	15.69	6.65	6.99	27.19	27.68	273.56	276.82
62	144.56	51.49	2	23.35	6.29	6.89	40.53	40.82	203.56	204.08
63	147.3	57.48	2	18.9	7.48	8.18	32.76	33.22	263.62	265.78
64	195.58	99.73	0.708	19.2	7.41	7.50	33.31	33.76	234.33	236.29
65	140	54.17	1.42	14.98	4.57	4.42	25.96	26.44	261.18	264.38
66	140	40	2.83	16.57	6.53	6.52	28.72	29.15	260.01	262.39
67	180.23	87.25	0.708	19.85	5.63	5.38	34.45	34.90	207.65	209.42
68	181.44	59	1.42	27.85	7.73	7.42	48.37	48.66	194.23	194.65

Table 4: Results of the optimization and verification for two objectives

SOLUTION ID	PARETO OPTIMAL SOLUTIONS				OBJECTIVES (PARETO OPTIMAL FRONT)			
					EFFECTIVE PIXEL SIZE (µm)		UNSHARPNESS(µm)	
	Voltage (kV)	Current (µA)	Exposure Time (second)	Source Sample Distance (cm)	Optimization	Experimental verification	Optimization	Experimental verification
1	152.45	50.76	0.708	27.81	48.37	48.60	145.46	145.81
2	170.88	78.9	0.5	35.73	62.21	62.21	124.59	124.42
3	185.26	84.85	0.5	49.55	86.39	86.39	86.39	86.39
4	140	44.92	0.267	14	24.23	24.75	244.09	247.52
5	140	40	1	24.42	42.42	42.64	170.31	170.58
6	140	43.64	2	19.85	34.45	34.57	207.65	207.43
7	140	40	0.5	21.59	37.49	37.63	188.21	188.15
8	140	40	0.267	17.89	31.03	31.20	218.34	218.41
9	140	40	0.267	16.12	27.91	28.29	224.85	226.31